

Multi-point Thoracic Deflection Measurement as a Predictor of Rib Injury in Frontal Collision

D. Bose¹, B. Pipkorn², J. R. Crandall¹, D. J. Lessley¹ and M. J. Trowbridge¹

¹ University of Virginia Center for Applied Biomechanics, Charlottesville, USA

² Autoliv Research, Vårgårda, Sweden

This paper has not been screened for accuracy nor refereed by any body of scientific peers and should not be referenced in the open literature.

ABSTRACT

Historically, anthropometric test devices (ATDs) designed to predict the risk of thoracic skeletal injuries in frontal crashes have been limited in their ability to discriminate injury independent of the restraint environment. Efforts to improve the accuracy of the ATD-based injury risk functions include the consideration of multi-point thoracic deflection information capable of characterizing the overall deformation of the rib cage independent of the applicable restraint type. The most advanced ATDs in terms of thoracic instrumentation measure multi-axis deflection at four locations, right and left aspects on the 4th and the 8th ribs. The objective of the current study is to assess whether thoracic deflection as measured at four locations provide sufficient information to reliably predict rib injury risk for a range of realistic restraint loading patterns. The computational methodology used to answer the above research question first evaluates the ability of a human finite element (FE) torso model to reproduce regional stiffness characteristics of the thorax as observed in restraint tests involving post mortem test subjects (PMHS). The torso model was then dynamically loaded to a nominally injurious level of deflection by four restraint types (i.e., diagonal belt, distributed load impactor, steering wheel hub impactor and cross-over dual belt) to estimate the true strain distribution within the ribs for each restraint condition. Following the restraint simulations, the thoracic model was deformed using the four-point deflection information measured in the first simulation as the input. The error in peak strain estimation was determined between the true strain distribution resulting from the restraint induced deformation of the thorax and the matched simulation where the displacements at the four thoracic locations were used to deform the thorax. The simulation results indicated that although the torso model has been previously validated for overall restraint loading response the ability of the model to characterize regional loading response was comparatively less biofidelic. Consequently, the error in estimating the peak thoracic strain ranged from 9% to 44% depending on the restraint type; however, the

location of the true peak strain was accurately predicted in the simulations with four point deflection information. It is important to note that the deformation of the thorax using four point deflections is an extreme case of localized point loading and the estimated strain distribution is thereby susceptible to artifactual errors. While the results from the study reports on the strain error estimates for the worst-case scenario, a more realistic evaluation of the ATD's ability to predict rib injury risk may require thoracic boundary conditions to be more representative of the ATD characteristics including structural stiffness and material properties.

INTRODUCTION

Rib fracture injury is the most common form of skeletal thoracic injury, simply referred to as thoracic injury in this study, present in almost 94% of all seatbelt restrained occupants sustaining a severe or fatal injury in frontal collisions (Kent et al., 2008). The injury metrics measured by ATDs in the thoracic region in conjunction with well-defined injury risk curves, such as the ones compiled by the U.S. National Highway Traffic Safety Administration (NHTSA) (Eppinger et al., 1999), provide a meaningful tool to estimate the risk of thoracic injuries in the real-world traffic conditions. Currently, injury metrics based on thoracic deflections measured by the ATD are in use to quantify the risk of thoracic injury; however, the associated injury risk curve may have limited ability to discriminate injury from non-injury when different restraint loading types and additional occupant parameters including age, gender and anthropometry are considered as explanatory variables for injury prediction (cf. Kent & Patrie, 2005).

Posterior deflection of the mid-sternum relative to the spine, commonly referred to as chest deflection, is measured by current frontal impact ATDs such as the Hybrid III dummy. Matched-pair comparisons involving ATD tests and PMHS have shown that the chest deflection measure can be used as an indicator of the risk of thoracic injury (Kent et al., 2001). Sternum deflection measures in the dummy, however, characterize the thoracic deformation at the mid-sternum location which, depending on the restraint type, may not correspond to the location of the maximum thoracic deflection. Kuppa & Eppinger (1998) analyzed results from 71 PMHS sled tests involving five different restraint conditions and suggested that maximum deflection occurred at the mid-sternum in only 25% of the total cases which lead the authors to conclude that maximum mid-sternum chest deflection alone was not a sufficient predictor of thoracic injury risk in comparison to the maximum of deflections recorded at multiple thoracic locations. To confirm the sensitivity of chest deflection as an injury predictor to the applicable restraint type, a pilot study was performed by the authors on the matched-pair sled test results involving the 50th percentile Hybrid-III adult male ATD and PMHS (for details on match-pair test conditions refer to Appendix Table A. 1). The results of the pilot study indicated that the risk of severe thoracic injury (score of three or more on the Abbreviated Injury Scaling (AIS, AAAM 2005) depends on the restraint type and the variation of deflection level for 50% risk can be as wide as 25 mm (Figure 1).

With advances in ATD sensor technology, thoracic deformation can be evaluated at multiple locations which should considerably improve the ability of the ATD to distinguish injury under different loading conditions. THOR (Test device for Human Occupant Restraint), an advanced frontal impact ATD developed by NHTSA, has the sensor capability to evaluate multi-dimensional anterior-posterior deflection of the thorax at four different locations (Figure 2) (Rangarajan et al., 1998). To compare the sensitivity in injury prediction between multi-point thoracic deflection and fixed-point chest deflection to different restraint conditions, a matched-pair test analysis involving multi-point deflection measured on the THOR ATD and the PMHS injury outcome was performed. Similar to the results obtained with chest deflection as an injury predictor, the correlation between the magnitude of maximum thoracic deflection measured at any of the four locations on the THOR, C_{max} , and the risk of severe thoracic injury, was also sensitive to the restraint type (Figure 1) (for details on match-pair test conditions refer to Appendix Table A.2). It should be noted that a relatively smaller sample size ($n= 29$) was available to develop the injury risk function for the THOR ATD measurements with restraint type as one of the covariates. Overall, matched-pair analysis involving both Hybrid-III and THOR ATD has confirmed that thoracic deflection measured at a single location on the ATD thorax is not sufficient to predict the risk of injury independently of the restraint type.

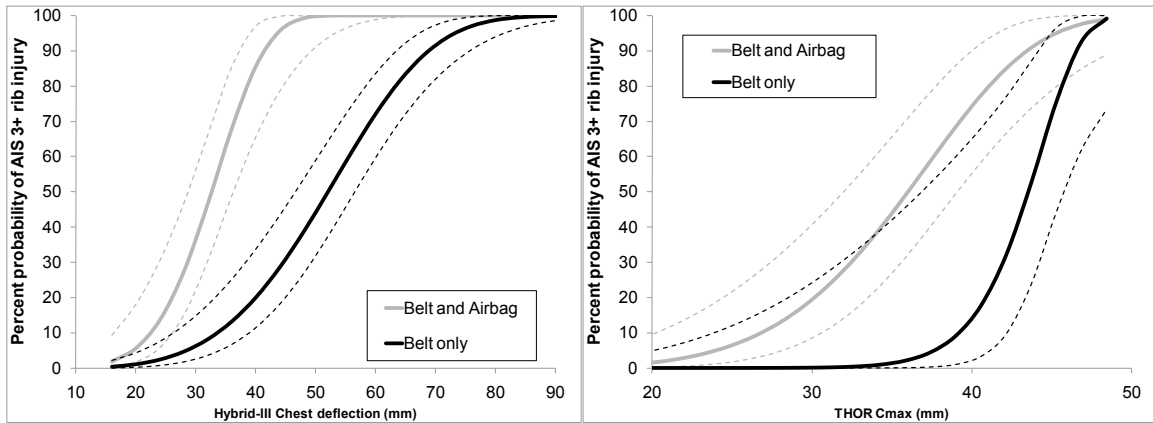


Figure 1: Sensitivity of the thoracic injury risk curve (for AIS 3+ rib injury) to restraint conditions based on matched-pair PMHS ATD sled test data. Figure on the left is based on tests involving Hybrid-III 50th percentile adult male ATD while the same of the right is based on tests involving the THOR ATD. The figures are based on right-censored parametric (Weibull distribution) survival analysis (Maximum likelihood estimates) with superimposed 95% confidence interval (dashed lines) for each of the restraint types.

Towards the development of an ATD-based thoracic injury function, current efforts focus on two necessary requirements: ATD instrumentation that estimates the peak of overall thoracic deformation based on multi-point deflection measurements and, secondly, identification of an injury predictor variable derived from deflection measurements such that injury prediction is insensitive to the nature of restraint loading. Factors that prevent multi-point deflection measures such as C_{max} from being a suitable injury predictor relate to the fact that C_{max} is a one-dimensional scalar quantity measuring the magnitude of deflection at only one location on the thorax. The contribution of resultant deflection, which includes deflections along the non-principal directions of loading (inferior-superior and lateral directions), and the coupling-interaction between the different regions of the rib-cage related to the overall thoracic deformation has been previously discussed (Shaw et al., 2007). In addition, the temporal characteristics of the deflections measured at multiple locations, rather than just their peak magnitudes, may provide better insight into instantaneous overall deformation pattern of the chest which, in turn, may relate to the risk of thoracic injury. In the current study, it is assumed that the risk of rib injury as predicted by the ATD will be dependent on the ability to correlate the peak strain in the rib cage when loaded under standard restraint conditions. Given that the most advanced ATD instrumentation currently available measures thoracic deflection at four distinct locations, the error between the peak thoracic strain as estimated by the ATD four measurement locations and the true peak thoracic strain was investigated.



Figure 2: Anterior view of the THOR ATD thorax structure with the locations of the multi-dimensional deflection sensor shown in hatched circles at the left and right aspect of the fourth and the eighth ribs.

Based on the above discussion the goal of the current study was to answer the research question of whether the multi-axial deflections measured at the four locations by the THOR ATD provides sufficient

information to accurately estimate the peak thoracic strain as produced by different restraint loading types. In order to answer that question, the current study focused on a computational methodology to predict the error in peak thoracic strain estimation by four-point deflection instrumentation when the thorax is loaded by standard restraint types. While several industry-standard computational models of the human thorax are currently in use, the deformation response of these thorax models have been validated primarily for the overall force deflection response using different restraint types (e.g., Murakami et al., 2004). For the purposes of this study it is necessary that the thorax model used to predict the strain be validated for regional stiffness response and the coupling interaction between different parts of the rib-cage structure. Summarizing, the objectives of the study towards the overall goal of the study are described as follows:

1. To evaluate the computational model of the human torso in terms of regional stiffness and coupling interaction between the different regions of the thorax.
2. To evaluate the error in the estimation of the peak strain in the thorax by a four-point deflection instrumentation and compare the range of this error across different restraint loading types.

METHODS

A previously validated finite element (FE) model of the human torso was used to evaluate thoracic deformation in response to loading conditions representative of four different vehicle restraint types: diagonal shoulder belt, frontal airbag represented as distributed load, steering wheel hub impactor at mid-sternum level and cross-over dual belt. The validity of the torso model for its regional thoracic deformation response was evaluated using results from experimental tests involving PMHS specimens. Further, a simulation matrix involving deformation of the thorax under matched boundary conditions was performed to estimate the error in peak strain estimation for each of the restraint types. The validation of the torso model and the estimation of peak strain using the simulation matrix are described in the following subsections.

Human torso model

Description of the torso model. The computational model of the human torso used in this study was obtained from the THUMS (Total Human Model for Safety) FE model of the whole human body, developed and validated by the research team at Toyota Central R&D Labs, Inc., to simulate the human response to impact loads (Oshita et al., 2002). The anthropometry measures of the THUMS model are representative of the 50th percentile American adult male. The model includes detailed anatomical features including skeletal structures, soft tissue organs, muscle groups and skin structure modeled using a total of over sixty thousand nodes and eighty thousand elements. The thorax region of the THUMS model consists of the sternum, ribs, clavicles, and the scapula modeled using deformable elements while vertebrae are modeled as rigid-bodies. The cortical and trabecular bones are distinguished in terms of material property and modeled with shell and solid elements, respectively. The internal soft tissue organs were modeled as deformable solid elements with simplified geometrical properties. The computational time step for the thorax model is of the order of 1.0e-8 seconds. Further details about the THUMS thorax model are available in Murakami et al. (2004).

Evaluation of the regional deformation response. The thorax region of the THUMS model has been previously validated for force-deflection response under different compressive restraint loading conditions using matched-condition data from PMHS subjects (Oshita et al., 2002; Murakami et al., 2004). The study by Murakami et al. (2004) validated the thoracic response of the model in a table-top restraint loading setup and further concluded that the model was capable of simulating the equivalent response of the human thorax in terms of sensitivity of the sternum stiffness to the restraint loading condition. While both ATD and computational model validation has been primarily focused on the overall stiffness response of the thorax to various restraint conditions, the coupled-interaction between the different regions of the thorax in response to a locally applied load is relatively less investigated (Shaw et al., 2007). The biofidelity of the torso model to accurately predict regional deformation characteristics and coupling between the different sub-structures of the thorax is necessary for the accurate prediction of rib fracture injury risk.

The experimental tests performed by Shaw et al. (2007) provided the data on three-dimensional deflections measured at multiple locations on five PMHS thoracic specimens in response to localized indenter loading and was used in the current study to validate the regional dynamic response of the torso model. The average age at death, stature, mass and chest depth for the five PMHS subjects were 63 years,

1.76 m, 72.2 kg and 20.2 cm, respectively. To replicate the PMHS test conditions, the denuded torso model with fixed displacement boundary conditions at the spine was loaded in the anterior-to-posterior direction with a rigid 62 X 62 mm indenter at three locations (lower left, mid-sternum, upper right) along the driver-side shoulder belt loading path. The three-dimensional deflections as a response to the indenter loading was estimated at ten marker locations on either aspect of the thorax and on the sternum at multiple rib levels (Figure 3). The dynamic loading rate of the indenter was approximately 1 m/s with a maximum stroke length of 30 mm to represent realistic non-injurious belt loading applicable to frontal collisions (Shaw et al., 2007).

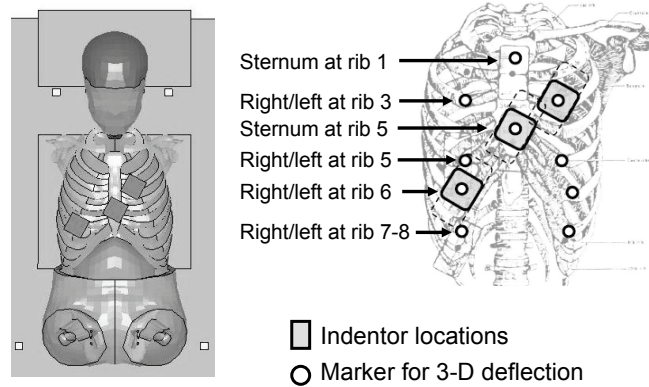


Figure 3: The anterior view of the torso model set-up for the validation of regional deflection response (left). The schematic on the right shows the lower right, middle and the upper left locations of the indenter and three dimensional deflection markers on the anterior thorax.

The evaluation of the torso model for regional deflection characteristics was comparable to that performed for the experimental study and included comparing the relative stiffness at each of the indenter locations and the regional relative deflections measured at multiple marker locations on the thorax. The regional stiffness of the torso model, expressed as the force-deflection time-history along the anterior-posterior (i.e., sternum-spine) direction and measured by the indenter, was compared to the measured response for each of the PMHS specimens at three indenter loading locations. The comparison of relative deflections at each marker location was done by calculating a normalized deflection measure based on the maximum indenter deflection for any of the indenter locations (Eq. 1). The normalized deflection at the 10 marker locations was then compared between the experimental results and model prediction.

$$\text{Normalized deflection} = (\text{maximum deflection at marker location}) / (\text{maximum indenter deflection}) \quad (1)$$

Strain estimation

Matched simulation matrix. Towards the second objective of evaluating the error in predicting the peak strain in the thorax using a four-point deflection instrumentation, a simulation matrix involving matched deformation simulations of the torso model was used. The matched simulations consist of estimating the overall deformation and the peak strain in the thorax for two sets of loading conditions involving a particular restraint type. The first set of conditions, referred to as the restraint loading type, estimates the true strain distribution in the thorax by loading the thorax using a restraint model with realistic geometry and boundary conditions. The results of the restraint loading type simulation include data on the three-dimensional deflection time history as measured by the four-point deflection instrumentation in addition to the estimation of the strain distribution. The second set of simulation condition, referred to as the deflection-controlled loading, estimates the strain distribution in the thorax by deforming the thorax using the multi-point deflection information obtained from the restraint loading simulation. The peak principal strain magnitude estimated on the thoracic skeletal structure by the two matched-pair simulations were compared to evaluate the error in peak strain estimation by the four-point deflection instrumentation for a particular restraint type. The range of error was evaluated by performing the matched-pair simulations for each of the four restraint types. A summary of the overall methodology is presented in Figure 4.

Model setup and boundary conditions. To perform the matched simulation matrix, the validated torso model was oriented in the supine posture, similar to the orientation used for validating the regional response, with fixed displacement boundary conditions to the spine and the pelvic structure (Figure 5). The torso-back and the head were positioned against two planar structures at different levels to ensure stability with no anterior-posterior movement of the spinal structure due to the inertial forces of the head/neck complex and the pelvis structure. The geometrical orientation of the THOR four-point deflection instrumentation with respect to the anatomical features was used to replicate a similar four-point deflection measurement system on the torso model. Two local coordinate systems (LCS) were identified on either aspects of the 4th and the 8th rib at a lateral distance of 72 mm and 126 mm, respectively, from the sternum centerline. The local coordinate systems were oriented such that local deflections at the 4th and the 8th rib were measured relative to the T11 and L2 vertebrae, respectively, on the spine. Simplified finite element models of the four restraint types-driver side diagonal shoulder belt, deformable planar structure for distributed loading, rigid hub and cross-over dual belt-represented using deformable shell elements were used in the restraint loading simulation of the thorax (Figure 5). The kinematic boundary condition for the restraints to simulate a dynamic deformation of the thorax includes a constant velocity (1 m/s) displacement pulse with peak stroke of 46 mm corresponding to chest compression of 23% of its initial depth under diagonal belt loading. The choice of restraint kinematics relates to a nominal risk of sustaining rib fracture injuries from a belt restraint loading in a 48 km/hr frontal collision (Kent et al., 2004). The kinematic boundary conditions were applied to the restraint attachment points in the anterior-to-posterior direction of the torso model.

RESULTS

Evaluation of the regional deformation response. The comparison of the regional stiffness response as estimated by the torso model at the three indenter locations with the PMHS test results is shown in Figure 6. The percent chest compression at the mid-sternum location relative to the initial chest depth was 8.2%, 20.6% and 5.3% for the upper left, mid-sternum and lower right indenter locations, respectively. While the force-deflection stiffness characteristics of the PMHS subjects were similar for all three indenter locations, the torso model stiffness measure was dependent on the indenter location. The normalized deflection measures at the ten marker locations that were estimated by the torso model were compared to the PMHS results and averaged for all five subjects (Table 1). Aggregating the cumulative error in the estimation of normalized deflections across all the ten marker locations, while the torso model response was most biofidelic for the lower right and the mid-sternum indenter locations the estimation at the upper left location was comparatively less biofidelic.

Comparison of peak strain estimation. The strain distribution and the peak strain magnitude were compared between the restraint loading and the deflection-control loading of the thorax for the four restraint types (Figure 7 and Table 2). The chest compression at the mid-sternum expressed as a percentage of the initial chest depth varied from 23% to 33%. The peak principal strain in the thoracic skeletal structure ranged from 0.7% to 3% as a result of loading by the four restraint types (Table 3). While the strain distribution due to restraint loading exhibited spatially continuous patterns that were distinct for each of the loading types, the strain distribution from deflection-controlled loading was localized in the region surrounding the peak strain location. Additionally, the deflection-control loading introduced high levels of strain in the regions where the displacement boundary condition was applied to deform the thorax. While the distributed loading resulted in the lowest value of peak strain among the four restraint types, the hub impactor produced highest values of localized strain at the point of contact with the thorax. In terms of predicting the magnitude and location of the peak strain, the error was minimum for the hub and the cross-over belt compared to the diagonal belt and the distributed load.

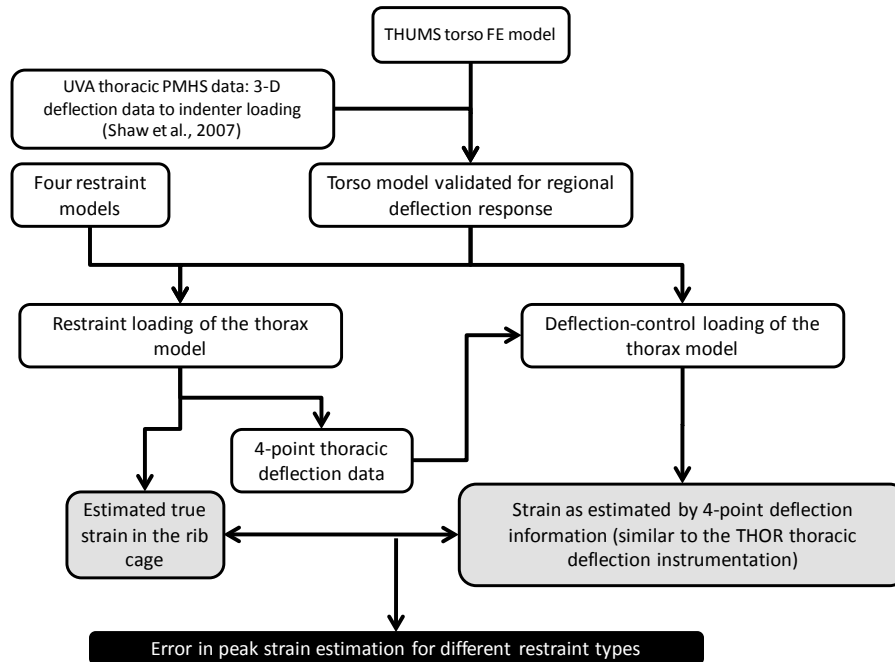


Figure 4: Overview of matched-pair simulation methodology

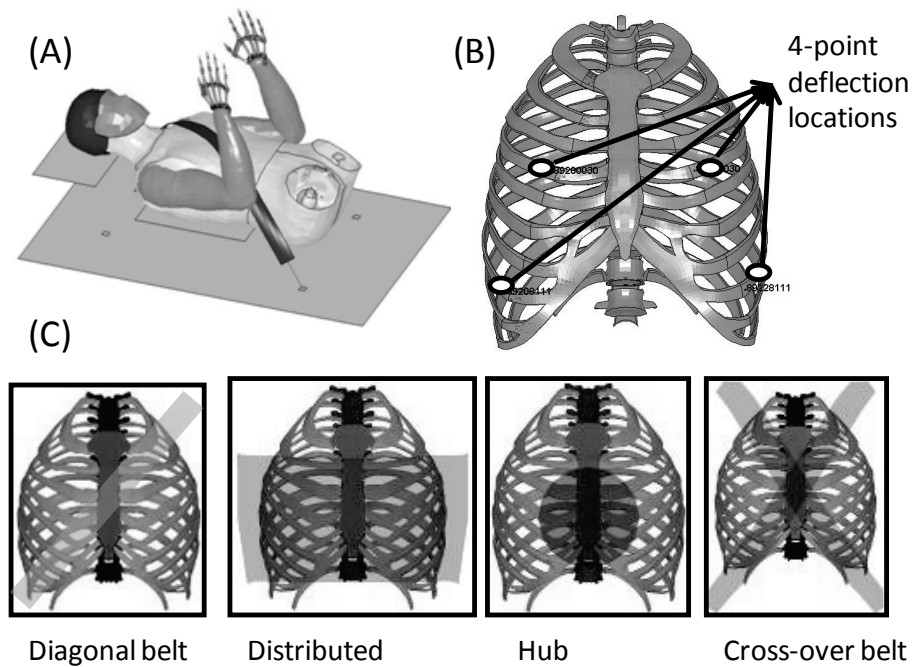


Figure 5: Overview of the torso model orientation and four different restraint types considered in this study. (A) shows the torso model oriented in a supine posture with the diagonal belt restraint type. (B) shows the four locations on the anterior rib cage of the torso model where the three-dimensional deflections were measured for the model corresponding to the geometry of the thoracic deflection instrumentation in the THOR ATD. (C) shows the loading region on the anterior thorax corresponding to each of the four restraint types.

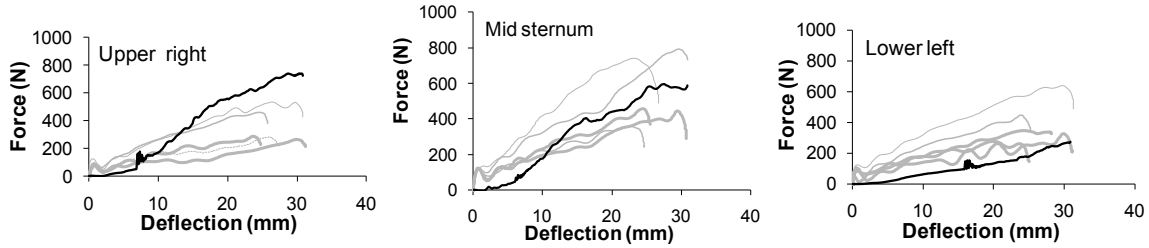
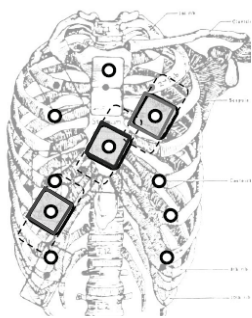


Figure 6: Regional stiffness response as estimated by the torso model compared with the PMHS stiffness response, as reported in Shaw et al., (2007), for three indenter locations along the diagonal belt loading path. For each loading location the grey curves represent the individual PMHS responses while the black curve represents the estimated model response.

Table 1. Normalized deflection at each of the 10 marker locations as estimated by the torso model compared with the PMHS results as reported in Shaw et al. (2007). For each of the tables the normalized deflection is reported if a marker was used in that location and the location of the indenter, where the normalized deflection is unity, is indicated by the grey cell. A value of unity for normalized deflection indicates highest degree of coupled deflection with respect to the indenter deflection and a value of zero indicates no coupling between the deflection at measured location and that of the indenter.



	Simulation			PMHS (average)			
	Right	Sternum	Left	Right	Sternum	Left	
Upper left	Rib loc.						
	S1		0.47		0.30		
	R3/L3	0.47		1.00	0.10	1.00	
	S5		0.88			0.40	
	R5/L5	0.35		0.74	0.10		0.30
	R6/L6	0.29		0.59	0.10		0.30
	R7-8/L7-8	0.21		0.38	0.10		0.20
Mid-sternum	Rib loc.						
	S1		0.35			0.20	
	R3/L3	0.50		0.50	0.30		0.40
	S5		1.00			1.00	
	R5/L5	0.41		0.41	0.50		0.50
	R6/L6	0.34		0.34	0.60		0.60
	R7-8/L7-8	0.20		0.20	0.50		0.50
Lower right	Rib loc.						
	S1		0.10			0.00	
	R3/L3	0.39		0.10	0.20		0.00
	S5		0.40			0.50	
	R5/L5	0.70		0.08	0.90		0.20
	R6/L6	1.00		0.06	1.00		0.30
	R7-8/L7-8	0.48		0.05	0.80		0.20

Figure 7: Comparison of principal strain distribution estimated at peak deformation for restraint loading and deformation control loading simulations.

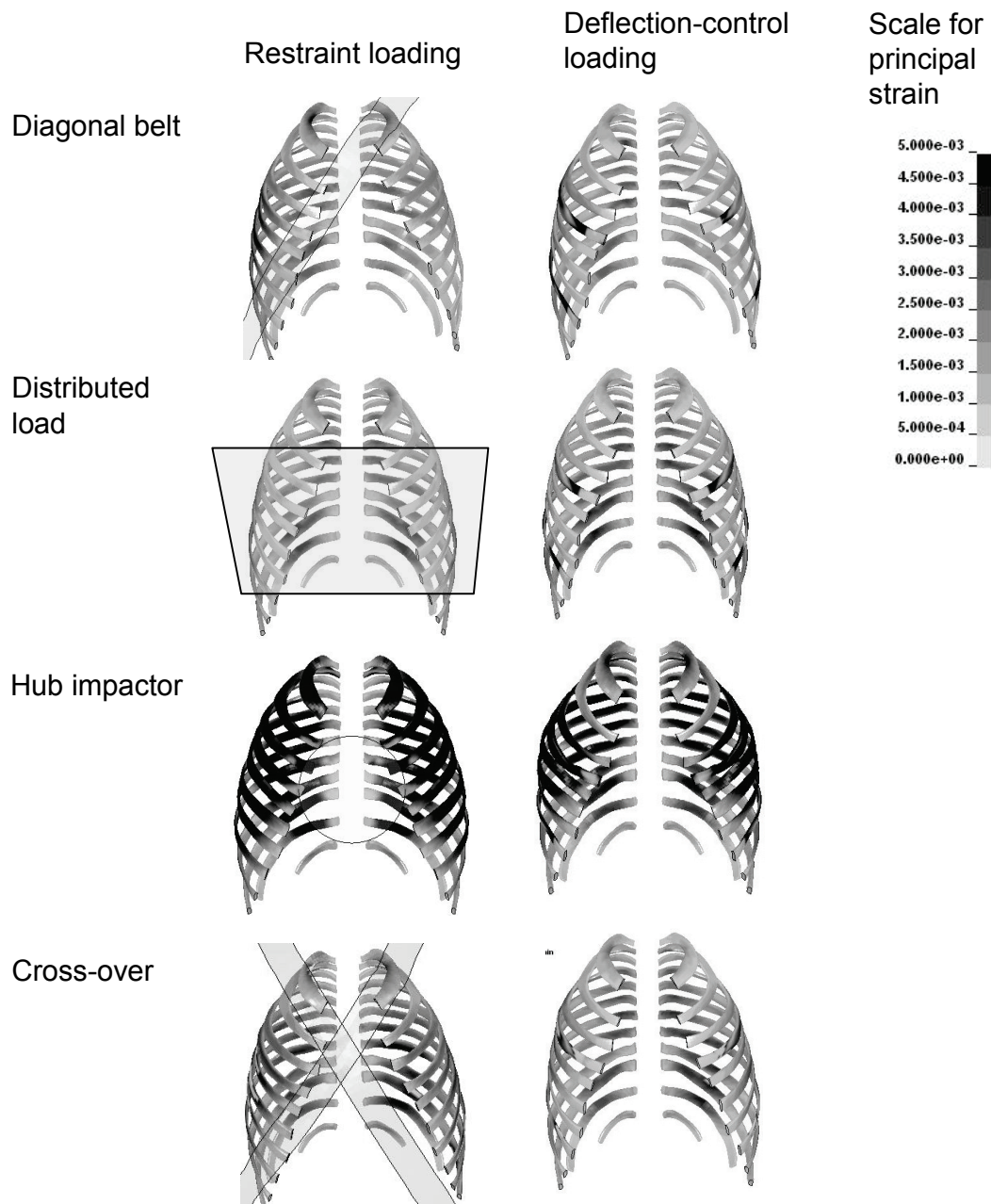
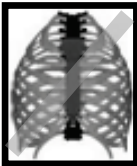
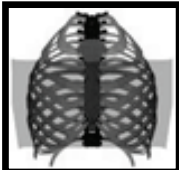
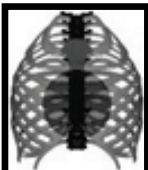


Table 2. Comparison of estimated principal strain at each rib location between the restraint type and the deflection-control type loading of the thorax by four different restraint types. The grey scale of the cells represents grading in terms of principal strain magnitude with white representing the minimum value of strain. All cells colored black represent indicate either strain was not measured (sternum and anterior 12th rib) or the strain estimated in displacement-control loading was erroneous due to localized deflection.

		Restraint loading					Deflection-control loading				
		Right aspect			Left aspect		Right aspect			Left aspect	
Ribs		Lateral	Anterior	S	Anterior	Lateral	Lateral	Anterior	S	Anterior	Lateral
1		0.007	0.002		0.002	0.005	0.003	0.001		0.001	0.000
2		0.003	0.001		0.001	0.004	0.002	0.001		0.001	0.001
3		0.003	0.003		0.003	0.003	0.002	0.001		0.001	0.001
4		0.005	0.001		0.003	0.003	0.004	0.004			0.002
5		0.007	0.005		0.002	0.003	0.005	0.002		0.002	0.002
6		0.009	0.004		0.002	0.004	0.004	0.002		0.002	0.002
7		0.008	0.003		0.001	0.004	0.005	0.001		0.001	0.003
8		0.008	0.003		0.000	0.004	0.013	0.002		0.006	0.003
9		0.006	0.004		0.000	0.003	0.005	0.003		0.000	0.000
10		0.007	0.004		0.000	0.003	0.005	0.003		0.000	0.002
11		0.004	0.000		0.000	0.003	0.005	0.000		0.000	0.002
12		0.003				0.001	0.003				0.001

		Restraint loading					Deflection-control loading				
		Right aspect			Left aspect		Right aspect			Left aspect	
Ribs		Lateral	Anterior	S	Anterior	Lateral	Lateral	Anterior	S	Anterior	Lateral
1		0.003	0.001		0.001	0.001	0.003	0.001		0.001	0.001
2		0.002	0.001		0.001	0.002	0.002	0.001		0.000	0.001
3		0.001	0.001		0.001	0.001	0.001	0.001		0.000	0.000
4		0.002	0.001		0.001	0.002	0.002	0.001			0.006
5		0.004	0.001		0.001	0.002	0.003	0.001		0.001	0.002
6		0.005	0.001		0.002	0.003	0.003	0.001		0.002	0.002
7		0.006	0.001		0.001	0.004	0.005	0.001		0.000	0.003
8		0.007	0.004		0.002	0.004	0.011	0.001			0.004
9		0.005	0.004		0.001	0.004	0.005	0.004		0.001	0.005
10		0.005	0.003		0.001	0.004	0.005	0.003		0.001	0.003
11		0.006	0.000		0.000	0.003	0.005	0.000		0.000	0.003
12		0.002				0.001	0.002				0.001

		Restraint loading					Deflection-control loading				
		Right aspect			Left aspect		Right aspect			Left aspect	
Ribs		Lateral	Anterior	S	Anterior	Lateral	Lateral	Anterior	S	Anterior	Lateral
1		0.009	0.005		0.004	0.003	0.007	0.002		0.002	0.002
2		0.007	0.022		0.003	0.008	0.010	0.010		0.003	0.002
3		0.035	0.030		0.013	0.035	0.006	0.006			0.032
4		0.003	0.003		0.007	0.011	0.029	0.017		0.017	0.025
5		0.025	0.025		0.015	0.030	0.020	0.019		0.019	0.006
6		0.019	0.022		0.025	0.011	0.016	0.005		0.004	0.007
7		0.017	0.009		0.005	0.017	0.010	0.003		0.014	0.005
8		0.005	0.009		0.002	0.016	0.005	0.003		0.001	0.003
9		0.006	0.006		0.001	0.007	0.005	0.002		0.000	0.005
10		0.004	0.003		0.001	0.019	0.004	0.000		0.000	0.004
11		0.006	0.000		0.000	0.013	0.002				0.001
12		0.001				0.001	0.002				0.001

		Restraint loading					Deflection-control loading				
		Right aspect			Left aspect		Right aspect			Left aspect	
Ribs		Lateral	Anterior	S	Anterior	Lateral	Lateral	Anterior	S	Anterior	Lateral
1		0.008	0.001		0.002	0.005	0.005	0.003		0.001	0.001
2		0.004	0.002		0.002	0.005	0.002	0.001		0.001	0.001
3		0.004	0.001		0.003	0.004	0.002	0.002		0.000	0.000
4		0.003	0.001		0.003	0.004	0.002	0.002			0.006
5		0.007	0.005		0.004	0.005	0.005	0.003		0.001	0.003
6		0.009	0.005		0.005	0.005	0.004	0.003		0.003	0.003
7		0.010	0.003		0.001	0.005	0.005	0.001		0.001	0.004
8		0.007	0.004		0.001	0.006	0.009	0.001		0.005	0.005
9		0.006	0.004		0.002	0.006	0.004	0.003		0.001	0.006
10		0.005	0.003		0.002	0.004	0.004	0.003		0.001	0.004
11		0.005	0.000		0.000	0.004	0.005	0.000		0.000	0.003
12		0.002				0.001	0.003				0.001

Table 3. Comparison of thoracic deformation measures estimated by the matched-pair simulation matrix for the four restraint types considered in this study.

<i>Peak strain comparison</i>	Diagonal belt	Distributed	Hub indenter	Cross-belt
Peak strain in restraint loading	0.009	0.007	0.035	0.010
Location of peak strain (rib no./aspect)	6 / right (lateral)	8 / right (lateral)	3 / left (lateral)	7 / right (lateral)
Peak strain in displacement control loading	0.013	0.010	0.032	0.009
Error in strain estimation (%)	44	43	9	10
Mid-sternum chest compression (%)	23.6	26.4	32.7	26.2
<i>Four-point deflection measures</i>				
Upper left deflection- x direction (mm)	19.15	30.56	110.42	32.52
Upper left deflection- Resultant (mm)	22.07	33.58	111.87	34.07
Upper right deflection- x direction (mm)	36.89	31.08	109.79	40.27
Upper right deflection- Resultant (mm)	43.29	34.49	111.11	43.39
Lower left deflection- x direction (mm)	9.24	37.48	24.4	39.31
Lower left deflection- Resultant (mm)	25.09	39.22	25.29	41.15
Lower right deflection- x direction (mm)	30.01	38.13	24.42	34.31
Lower right deflection- Resultant (mm)	42.54	40.88	25.18	38.26
Cmax - x direction (mm)	36.89	38.13	110.42	40.27
Location of Cmax - x direction	Upper right	Lower right	Upper left	Upper right
Cmax - Resultant (mm)	43.29	40.88	111.87	43.39
Location of Cmax – Resultant	Upper right	Lower right	Upper left	Upper right
Average of 4-point deflection - Resultant	33.25	37.04	68.36	39.22

DISCUSSION

While previous studies have used a single location of deflection measures (e.g., chest deflection and C_{max}) for thoracic injury prediction, a pilot analysis performed on matched-pair PMHS ATD sled test results has confirmed that ATD-based risk curves are sensitive to the restraint loading condition. To remove the dependency on restraint condition as an explanatory variable, it is desirable that the injury predictor, a scalar or vector of multi-point deflections, provide sufficient information to characterize the overall thoracic deflection for all restraint types and that explicit information on restraint type is not necessary for injury prediction. Towards that goal, the advanced frontal collision ATD, THOR, includes a multi-axial four-point thoracic deflection instrumentation to provide time-histories of regional deflection characteristics on the anterior thorax. While efforts are underway to analyze the multi-point deflection data and derive restraint-independent injury risk curves, it is of interest to investigate whether deflections as measured by the THOR instrumentation provide sufficient information to reliably estimate the location of peak strain in the human thorax for a range of realistic restraint loading pattern. To answer the above research question, the current study reports on the findings of a simulation based study to evaluate the error in peak strain estimation in the thorax using deflection information from four locations.

While validation of the torso model in terms of overall thoracic response to different restraint types has been reported in the literature, the ability of the model to accurately simulate deformation characteristics in response to regional loading had not been previously verified. The stiffness characteristics of the torso model matched the PMHS response-set at the mid-sternum indenter location but did not reproduce the stiffness at the indenter locations for the lower right and upper left regions of the thorax. This indicates that the coupled deflection responses of the torso model were not biofidelic when the sternum was not directly loaded and, thus, a difference in the effective stiffness of the thorax was observed between the PMHS response set and the model response. When normalized deflection measured at multiple rib locations was

compared between the simulation and the PMHS test results, a similar sensitivity to the indenter location was observed. Normalized deflection (Eq. 1) takes a value of unity when the marker location is perfectly coupled in terms of deflection magnitude with the indenter location and similarly a value of zero is indicative of the marker location to be completely decoupled with the indenter location. For the indenter location upper right, which among the three locations reported highest value of cumulative error in estimated normalized deflection, it appeared that the marker locations further away from the indenter were significantly more coupled in the model response when compared to the PMHS response set. Furthermore insight into the costal-cartilage joint properties and modeling and contact interaction between the indenter and the rib structures may improve the biofidelity of the regional response estimated by the model.

Towards the second objective, the torso model was used to estimate strain for each restraint type for two sets of matched simulation conditions—restraint loading and deflection-control loading—as described in the study. The strain estimated under restraint loading was indicative of the true strain field in the rib cage and the region for the highest value of estimated principal strain was similar to the region with most frequent rib fractures in matched experimental test conditions (Crandall et al., 2000). The simulation results for restraint loading conditions showed that the rib location and aspect corresponding to the peak principal strain were in agreement with the location of the measured C_{max} (for both uni-axial and resultant measurements) in the model (except for the cross-over restraint where peak strain was measured at the right 7th rib and C_{max} was estimated at the upper right location although the difference in C_{max} -resultant measured at upper right and lower right was only 5 mm). The importance of accounting for deflections in the non-principal directions of loading (interior-superior and lateral anatomical directions) was emphasized in the results (Table 3) as the difference in between C_{max} measured in the anterior-to-posterior direction and the resultant C_{max} ranged between 1.2% (hub impactor) to 14.8% (diagonal belt).

The strain distribution produced by the deflection-control loading provided a reasonable estimate to the location of true peak strain, although, the error in the magnitude of estimated strain was as high as 44% which was observed in the case of the diagonal belt loading. Two important characteristics of the computational model may contribute to the overestimation of peak strain when the thorax was deformed using the deflection boundary conditions. First, as the deflection boundary conditions were applied to a localized set of nodes on the rib locations a high strain region was estimated around the nodes as an artifact due to the localized deflection. The magnitude of strain measured at the four deflection locations was consistently higher than the true peak strain measured in the matched restraint loading simulation for all loading types. Given that these deflections represent conditions with a nominal risk of rib injury, the peak strains observed in these simulations are approximately 1% in magnitude. For such low magnitudes of strain any artifact in the strain measurement due to localized deflection may overestimate the estimated error in peak strain. Secondly, as highlighted previously the coupled deflection response of the torso requires further adjustments to accurately predict regional deformation characteristics. Improving the torso model was beyond the scope of this study but it is suggested that based on PMHS regional stiffness and deformation data the component structures and the material properties may be tuned for improving the biofidelity of the response.

While the objective of the study was to evaluate the performance of the four-point deflection measurements to predict the peak strain in the human thorax, the implications of the results for developing an ATD based injury risk function must be realized. First, the true interpretation of the results is only applicable for the human thorax while taking into consideration the realistic geometry and material properties of the skeletal and soft-tissue structures. The range of error as predicted in this study reflects an extreme-case evaluation of the four-point deflection to predict the peak strain in the actual human thorax model. A similar comparison to evaluate the performance of four-point deflection measurements using an ATD model may yield substantially lower values of error estimation due to simplified geometry and relatively less compliant structures leading to smoother deformation gradients across the thoracic outer surface. While evaluating the true risk of rib injury requires thoracic deformation estimated in a human model, realistic characterization of ATD-based multi-point deflections requires boundary conditions at the measurement locations similar to the ATD structure rather than the relatively more compliant tissue structures. The human thorax model was chosen in this study to evaluate the maximum threshold of error in predicting peak strain or risk of rib injury considering the true boundary conditions and further assuming that the ATD instrumentation will be capable of replicating the deformation pattern as measured on the PMHS or any error in deformation estimation may be

compensated using statistical correlation methods. To gain further insight into the validity of this assumption, it is necessary to compare the true deformation contour of the human thorax with the deformation contours as observed on the ATD thorax using computational methods. The proposed task will highlight the accuracy of the ATD multi-point deflection measurements to characterize the effect of any localized deflections which may be observed in the human model as a result of restraint-loading conditions.

CONCLUSIONS

A computational methodology was used in this study to evaluate the error in peak strain estimation using four-point deflection instrumentation. The simulation results indicated that the deflection information measured at the four locations may accurately predict the location of the peak strain for loading due to standard restraint types. However, the error in the estimation of peak strain magnitude was approximately 10% for the hub impactor and the cross-belt restraints while the same was approximately 43% in the case of diagonal belt and distributed loads. To accurately estimate the error in the peak strain further insight into the model properties and improvements to the regional structural response is required. The robustness of the methodology to evaluate error in strain estimation may be further validated by considering different loading rates, higher values of chest compression and failure characteristics in the torso model. The validity of the model under the different conditions as described above will allow for the characterization of a multi-point deflection measure that may accurately predict the risk of rib injury independent of the applicable restraint conditions.

ACKNOWLEDGEMENTS

We would like to acknowledge NHTSA's Research and Development Program for providing both research direction and financial support. In particular we would like to thank Dr. Erik Takhounts at NHTSA for his guidance in designing the study and also would also like to thank Dr. Rich Kent, UVa Center for Applied Biomechanics, for his help on assimilating the experimental data and providing background insight on this topic.

REFERENCES

- AAAM (1990). The abbreviated injury scale -1990 revision (AIS 90). [report] Association for the Advancement of Automotive Medicine, Des Plains, IL.
- CRANDALL, J, KENT, R, PATRIE, J, FERTILE, J, MARTIN, P.,(2000) Rib fracture patterns and radiologic detection – a restraint-based comparison. Proc. of the Association for the Advancement of Automotive Medicine 44:235-59.
- EPPINGER, R., SUN, E., BANDAK, F. et al., (1999) Development of improved injury criteria for the assessment of advanced automotive restraint systems–II. [report] National Highway Traffic Safety Administration, U.S. Department of Transportation, Washington, DC.
- KENT, R. W., CRANDALL, J. R., BOLTON, J. R., et al., (2001) The influence of superficial soft tissues and restraint condition on thoracic skeletal injury prediction, *Stapp Car Crash Journal*, 45, pp. 183–203.
- KENT, R., CRANDALL, J., BOLTON, J., PRASAD, P., NUSHOLTZ, G., MERTZ, H., and KALLIERIS, D., (2001b). Restrained Hybrid-III dummy-based criteria for thoracic hard-tissue injury prediction. Proc. 2001 Conference of the International Research Council on Biomechanics of Injury conference (IRCOBI), Isle of Man.
- KENT, R., LESSLEY, D., SHERWOOD, C., (2004). Thoracic response to dynamic, non-impact loading from a hub, distributed belt, diagonal belt, and double diagonal belts. *Stapp Car Crash Journal*, 48.
- KENT, R. W. and PATRIE, J. T., (2005) Chest deflection tolerance to blunt anterior loading is sensitive to age but not load distribution. *Forensic Science International*, 149, 121-128.
- KENT, R. W., WOODS, W., and BOSTROM, O. (2008). Fatality risk and the presence of rib fractures. *Annual Proc. of the Association for the Advancement of Automotive Medicine*, 52, 73-82.

- KUPPA S. and EPPINGER, R., (1998). Development of an improved thoracic injury criterion, Stapp Car Crash Journal, pp. 139–153.
- MURAKAMI, D., KITAGAWA, Y., KOBAYASHI, S., KENT, R., and CRANDALL, J. (2004). Development and Validation of a finite element model of a vehicle occupant. Proc. Society of Automotive Engineers World Congress, Detroit, Michigan.
- OSHITA, F., OMORI, K., NAKAHIRA, Y., & MIKI, K. (2002). Development of a finite element model of the human body. 7th International LS-Dyna Users Conference, Nagoya, Japan. , 1 37-48.
- PETITJEAN, A., LEBARBE, M., POTIER, P., TROSSEILLE, X., LASSAU, J-P., (2002). Laboratory Reconstructions of Real World Frontal Crash Configurations using the Hybrid III and THOR Dummies and PMHS. Stapp Car Crash Journal, 46, pp. 27—54.
- RANGARAJAN, N., WHITE, R., SHAMS, T., BEACH, D., FULLERTON, J., HAFFNER, M. P., et al. (1998). Design and performance of the THOR advanced frontal crash test dummy thorax and abdomen assemblies. 16th International Technical Conference on the Enhanced Safety of Vehicles (ESV), Windsor, Canada.
- SHAW, G., LESSLEY, D., EVANS, J., CRANDALL, J., SHIN, J., PORTIER, P., PAOLONI, G. (2007). Quasi-static and dynamic thoracic loading tests: cadaveric torsos. Proc. of the International Research Council on Biomechanics of Injury conference (IRCOBI), Maastricht, Netherlands.

APPENDIX

A. Matched-pair test details

Table A. 1. Details of UVa matched-pair Hybrid-III PMHS tests. All tests were performed at the University of Virginia Center for Applied Biomechanics expect for the Test IDs with prefix MCW and UH which were performed at the Medical College of Wisconsin and University of Heidelberg, respectively (Kuppa and Eppinger, 1998, Kent et al., 2001b).

Test ID	Sled delta-V (km/h)	Restraint type	PMHS position	PMHS age (years)	PMHS sex	PMHS stature (m)	PMHS rib injury (AIS 3+)	Hybrid-III Chest deflection (mm)
53	34.8	Belt only	Driver	61	Female	1.53	1	50
55	38.1	Belt only	Driver	62	Female	1.76	1	74
61	47.0	Belt only	Driver	62	Male	1.72	1	44
66	47.0	Belt only	Driver	57	Male	1.69	1	44
102	33.8	Belt only	Driver	60	Male	1.76	1	57
103	33.8	Belt only	Driver	57	Male	1.79	1	57
104	33.8	Belt only	Driver	66	Female	1.79	1	57
113	46.8	Belt only	Driver	24	Female	1.59	1	75
114	46.8	Belt only	Driver	60	Female	1.64	1	75
173	24.6	Belt only	Driver	61	Male	1.67	1	56
174	24.6	Belt only	Driver	57	Female	1.68	1	56
175	24.6	Belt only	Driver	58	Male	1.85	0	56
223	53.4	Belt only	Driver	51	Male	1.69	1	64
224	53.4	Belt only	Driver	58	Male	1.75	1	64
225	53.4	Belt only	Driver	36	Male	1.77	1	64
227	53.3	Belt only	Driver	53	Male	1.65	1	64
228	53.3	Belt only	Driver	47	Male	1.77	1	64
229	53.3	Belt only	Driver	37	Male	1.83	1	64
250	54.1	Belt only	Driver	39	Male	1.77	1	57
252	58.9	Belt only	Driver	37	Male	1.77	1	59

257	56.5	Belt only	Driver	33	Male	1.79	1	52
258	56.5	Belt only	Driver	69	Male	1.78	1	52
259	56.5	Belt only	Driver	64	Female	1.63	1	52
294	56.8	Belt only	Driver	68	Female	1.48	1	37
295	56.8	Belt only	Driver	57	Male	1.87	1	37
296	56.8	Belt only	Driver	59	Male	1.81	1	37
303	57.5	Belt and airbag	Driver	64	Male	1.54	0	31
304	57.5	Belt and airbag	Driver	65	Male	1.68	1	31
305	57.5	Belt and airbag	Driver	66	Female	1.61	1	31
333	58.2	Belt and airbag	Driver	51	Male	1.70	1	30
334	58.2	Belt and airbag	Driver	49	Male	1.86	1	30
335	58.2	Belt and airbag	Driver	50	Male	1.72	0	30
411	57.0	Belt and airbag	Driver	60	Male	1.72	1	25
412	57.0	Belt and airbag	Driver	70	Male	1.78	1	25
533	48.6	Belt and airbag	Driver	67	Female	1.63	0	27
534	48.6	Belt and airbag	Driver	47	Male	1.70	1	27
535	48.6	Belt and airbag	Driver	57	Female	1.63	1	27
544	48.6	Belt and airbag	Driver	59	Female	1.68	1	27
545	48.6	Belt and airbag	Driver	67	Male	1.76	0	27
577	47.6	Belt and airbag	Front passenger	57	Male	1.74	0	29
578	47.6	Belt and airbag	Front passenger	69	Female	1.55	1	29
579	47.6	Belt and airbag	Front passenger	72	Female	1.56	1	29
580	47.6	Belt and airbag	Front passenger	57	Female	1.77	0	29
647	56.4	Belt and airbag	Front passenger	63	Male	1.75	1	16
665	48.0	Belt and airbag	Front passenger	55	Male	1.76	0	40
666	48.0	Belt and airbag	Front passenger	69	Male	1.76	0	40
667	48.0	Belt and airbag	Front passenger	59	Female	1.61	1	40
668	48.0	Belt and airbag	Front passenger	54	Female	1.62	1	40
1094	29.4	Belt only	Front passenger	49	Male	1.78	0	23
1095	29.4	Belt only	Front passenger	44	Male	1.72	0	23
1096	29.4	Belt only	Front passenger	39	Male	1.84	0	23
1262	48.0	Belt only	Rear passenger	51	Male	1.75	1	33
1263	48.0	Belt only	Rear passenger	57	Female	1.65	1	33
1264	48.0	Belt only	Rear passenger	57	Male	1.79	1	33
UH9013	48.0	Belt only	Driver	34	Male	1.80	0	25
MCW105	49.0	Belt only	Driver	67	Male	1.75	1	27
MCW102	49.7	Belt only	Driver	57	Male	1.78	1	39
MCW104	51.8	Belt only	Driver	58	Male	1.78	1	29
MCW101	50.8	Belt only	Driver	58	Male	1.80	1	34
MCW103	50.0	Belt only	Driver	66	Male	1.78	1	40

Table A. 2. Details of UVa matched-pair THOR PMHS tests. All tests were performed at the University of Virginia Center for Applied Biomechanics except for the Test IDs with prefix FR which were performed by Petitjean et al., 2002.

Test ID	Sled delta-V (km/h)	Restraint type	PMHS position	PMHS age (years)	PMHS sex	PMHS stature (m)	PMHS rib injury (AIS 3+)	THOR Cmax (mm)
650	48	Belt only	Front passenger	40	Male	1.50	0	14.2
651	48	Belt only	Front passenger	70	Male	1.76	0	14.2
652	48	Belt only	Front passenger	46	Male	1.75	0	14.2
1294	48	Belt only	Front passenger	76	Male	1.76	1	39.1
1295	48	Belt only	Front passenger	47	Male	1.76	1	39.1
1094	29	Belt only	Front passenger	49	Male	1.61	0	24.9
1095	29	Belt only	Front passenger	44	Male	1.74	0	24.9
1096	29	Belt only	Front passenger	39	Male	1.55	0	24.9
1262	48	Belt only	Front passenger	51	Male	1.56	1	45.6
1263	48	Belt only	Front passenger	57	Female	1.77	1	45.6
1264	48	Belt only	Front passenger	57	Male	1.78	1	45.6
665	48	Belt and airbag	Front passenger	55	Male	1.77	1	32.9
666	48	Belt and airbag	Front passenger	69	Male	1.78	1	32.9
667	48	Belt and airbag	Front passenger	59	Female	1.72	1	32.9
577	48	Belt and airbag	Front passenger	57	Male	1.84	0	33.0
578	48	Belt and airbag	Rear passenger	69	Female	1.75	1	33.0
579	48	Belt and airbag	Rear passenger	72	Male	1.65	1	33.0
580	48	Belt and airbag	Rear passenger	57	Female	1.79	0	33.0
1386	48	Belt and airbag	Rear passenger	67	Male	1.75	1	35.8
1387	48	Belt and airbag	Rear passenger	69	Male	1.71	0	35.8
1389	48	Belt and airbag	Rear passenger	72	Male	1.75	1	35.8
FR05	64	Belt and airbag	Driver	78	Female	1.69	1	42.5
FR22	64	Belt and airbag	Driver	81	Male	1.74	1	42.5
FR17	64	Belt and airbag	Driver	76	Male	1.72	1	44.0
FR23	64	Belt and airbag	Driver	75	Male	1.69	1	44.0
533	48	Belt and airbag	Driver	67	Female	1.63	0	24.5
534	48	Belt and airbag	Driver	47	Male	1.75	1	24.5
544	48	Belt and airbag	Driver	59	Female	1.69	1	24.5
545	48	Belt and airbag	Driver	67	Male	1.84	1	24.5